

Residual Diffusion Models for Variable-Rate Joint Source Channel Coding of MIMO CSI

Sravan Kumar Ankireddy, Heasung Kim, Hyeji Kim
Department of Electrical and Computer Engineering
The University of Texas at Austin

Abstract—Despite significant advancements in deep learning-based CSI compression, some key limitations remain unaddressed. Current approaches predominantly treat CSI compression as a source coding problem, neglecting transmission errors. In finite block length regimes, separate source and channel coding proves suboptimal, with reconstruction performance deteriorating significantly under challenging channel conditions. While existing autoencoder-based compression schemes can be readily extended to support joint source-channel coding, they struggle to capture complex channel distributions and exhibit poor scalability with increasing parameter count. To overcome these inherent limitations of autoencoder-based approaches, we propose Residual-Diffusion Joint Source-Channel Coding (RD-JSCC), a novel framework that integrates a lightweight autoencoder with a residual diffusion module to iteratively refine CSI reconstruction. Our flexible decoding strategy balances computational efficiency and performance by dynamically switching between low-complexity autoencoder decoding and sophisticated diffusion-based refinement based on channel conditions. Comprehensive simulations demonstrate that RD-JSCC significantly outperforms existing autoencoder-based approaches in challenging wireless environments. Furthermore, RD-JSCC offers several practical features, including a low-latency 2-step diffusion during inference, support for multiple compression rates with a single model, robustness to fixed-bit quantization, and adaptability to imperfect channel estimation.

Index Terms—Generative models, Diffusion models, Compression, CSI, JSCC, variable-rate compression

I. INTRODUCTION

As data transmission volumes continue to increase, massive multiple-input multiple-output (MIMO) has emerged as a fundamental technology for scaling next-generation wireless networks. By employing a large array of antennas at the base station (BS), multiple user equipment (UE) can achieve high-throughput communication, even under suboptimal channel conditions. However, achieving this requires accurate channel state information (CSI) to enable effective precoding for downlink transmission. In frequency division duplexing (FDD) systems, the uplink CSI is obtained via channel estimation, while the downlink CSI must be fed back from the user equipment (UE) in an efficient manner [1].

Deep learning (DL) has significantly advanced various areas within physical layer communication, including non-linear channel code design [2]–[6], neural channel decoding [7]–[12], and MIMO channel estimation [13]–[15]. This work focuses specifically on the challenge of *lossy compression* of CSI at

the physical layer. Traditional compression techniques, such as compressed sensing [16], do not work well CSI compression due to the lack of inherent sparsity in CSI structures, making deep learning a better alternative. The field of lossy compression using neural networks, commonly referred to as *neural lossy compression*, has gained considerable attention in applications such as image compression [17]–[19] and video compression [20]. More recently, similar methodologies have been leveraged to significantly enhance the efficiency of CSI compression [21], starting with CSINet [13], which achieved substantial improvements over the then state-of-the-art compressed sensing methods by leveraging convolutional neural networks (CNNs). This breakthrough led to a series of subsequent studies that further refined CNN-based compression techniques [22]–[26]. Further, similar approaches have been adapted for joint source channel coding (JSCC) of CSI [27].

Recently, neural image compression has witnessed a significant breakthrough in both compression efficiency and reconstruction quality with the adoption of diffusion models [28], [29]. Originally designed to generate novel images based on various conditioning variables, these models were rapidly adapted for image compression. In [30], the authors introduced a diffusion-based compression framework that reconstructs images through a reverse diffusion process conditioned on contextual information, outperforming certain GAN-based methods. Further, extremely low rate compression schemes have been proposed by leveraging the strong image priors of pretrained diffusion models [31]. Likewise, [32] utilized vector quantized generative adversarial networks (VQGANs), demonstrating the effectiveness of robust codebook priors for discrete visual feature representation in image synthesis, thus providing new insights for compression. More recently, [19] applied principal component analysis (PCA) to enable variable-rate compression, while [33] proposed leveraging spatial entropy [34] to learn latent representations at multiple resolutions, facilitating a continuous range of bitrates.

While diffusion models have been studied extensively in image compression space, their potential for CSI compression remains comparatively underexplored. A notable advancement in this direction is the generative diffusion-based CSI compression framework proposed in [35], demonstrating significant improvements over traditional autoencoder-based methods for modeling complex channels. Building upon this promising

*Under Review. Correspondence to: sravan.ankireddy@utexas.edu

foundation, our work aims to further enhance diffusion-based CSI compression in two key dimensions. First, we prioritize reconstruction fidelity by balancing output diversity, shifting the model’s objective from generating novel samples towards maximizing reconstruction accuracy. Second, we utilize a nested representation learning approach to simultaneously capture multiple compression levels within a unified latent space, enabling dynamic and graceful adaptation of the compression rate in response to fluctuating bandwidth constraints.

In this work, we propose a novel residual diffusion-based variable-rate CSI compression framework tailored for efficient compression of CSI matrices in massive MIMO systems. The proposed framework features an encoder leveraging a low-complexity convolutional neural network (CNN) architecture and a two-stage decoding process at the receiver. Specifically, the decoder comprises an initial CNN-based reconstruction stage followed by a U-Net-based diffusion refinement model, which iteratively enhances CSI reconstruction quality. The main contributions of this paper are summarized as follows:

- We propose a residual-diffusion-based formulation that enhances the CSI reconstruction by initializing the reverse diffusion with a coarse CSI estimate, rather than conventional random Gaussian noise.
- We propose a flexible two-stage decoding framework that adaptively switches between low-complexity autoencoder and high-fidelity diffusion-based decoders, based on channel conditions (Sec. IV).
- We validate the efficacy of our proposed method by comparing against state-of-the-art deep learning-based JSCC schemes for CSI compression, using the widely recognized COST2100 outdoor dataset [13] and 3GPP indoor dataset using QuaDRiGa [36] (Sec. V).
- We perform a systematic comparative study across multiple neural architectures and diverse channel scenarios, revealing that diffusion-based models significantly outperform autoencoder-based methods only when channel complexity is sufficiently high (Sec. VII-A).
- We adopt a nested representation learning framework to support multiple compression levels within a single model (Sec. VI) and support fixed-bit quantization of encoder-output for efficient storage and transmission (Sec. VII-C).

II. SYSTEM MODEL AND PROBLEM FORMULATION

In this work, we consider a massive MIMO system operating in frequency division duplex (FDD) mode, where a base station (BS) with N_t antennas communicates with a user equipment (UE) equipped with N_r antennas. Considering the large-scale nature of MIMO, we assume $N_t \gg 1$ and set $N_r = 1$ for simplicity. The downlink CSI is $H_d \in \mathbb{C}^{N_c \times N_t}$ and the uplink CSI is denoted by $H_u \in \mathbb{C}^{N_c \times N_t}$ in the spatial-frequency domain, where \mathbb{C} denotes the set of complex numbers and N_c is the number of subcarriers.

The encoder f_{enc} at the UE is designed to efficiently compress the high-dimensional channel measurement H_d into

a fixed-length representation $\mathbf{s} \in \mathbb{C}^k$. The compression rate is thus given by

$$r = \frac{k}{N_t \times N_c}.$$

The compressed representation can be transmitted on a noisy uplink channel using k subcarriers, while imposing an unit power constraint for the subcarriers $\frac{1}{k} \mathbb{E}[\mathbf{s}\mathbf{s}^*] = 1$. The received signal at the BS is processed using maximal ratio combining (MRC).

The compressed representation at the receiver is processed in two stages. First, the decoder f_{dec} reconstructs an estimate \hat{H}_d from the compressed representation \mathbf{s} , aiming to minimize distortion relative to the original input H_d . Next, to further refine the reconstruction, the noisy estimate \hat{H}_d is processed by a denoising diffusion model f_{den} , iteratively reducing the distortion using the reverse diffusion. Specifically, we use the residual diffusion formulation [37]. Following standard practice in CSI compression literature, we adopt mean squared error (MSE) as the distortion metric.

The encoder function is defined as $f_{\text{enc}} : H_d \mapsto \mathbf{s}$, while the decoder function is given by $f_{\text{dec}} : \mathbf{s} \mapsto \hat{H}_d$, and the denoising model operates as $f_{\text{den}} : \hat{H}_d \mapsto H'_d$. Given the encoder parameters θ_{enc} , the compressed representation \mathbf{s} is obtained as $\mathbf{s} = f_{\text{enc}}(H_d; \theta_{\text{enc}})$. Similarly, the decoder, parameterized by θ_{dec} , reconstructs an estimate of the target as $\hat{H}_d = f_{\text{dec}}(\mathbf{s}; \theta_{\text{dec}})$. Finally, the denoising model, governed by θ_{den} , further enhances the reconstruction, producing $H'_d = f_{\text{den}}(\hat{H}_d; \theta_{\text{den}})$. The complete set of model parameters is thus given by $\theta = (\theta_{\text{enc}}, \theta_{\text{dec}}, \theta_{\text{den}})$.

The learning process is designed to minimize the following objective function:

$$\theta^* = \arg \min_{\theta} \mathbb{E}_{P(H_d, H'_d)} [d(H'_d, f_{\text{den}}(f_{\text{dec}}(f_{\text{enc}}(H_d; \theta_{\text{enc}}); \theta_{\text{dec}}); \theta_{\text{den}}))] \quad (1)$$

where $d(\cdot, \cdot)$ represents a distortion metric that quantifies reconstruction quality. The parameters $\theta = (\theta_{\text{enc}}, \theta_{\text{dec}}, \theta_{\text{den}})$ are optimized using a two-stage training process, detailed in Sec. IV.

III. DEEP LEARNING FOR CSI COMPRESSION

In this section, we introduce a low-complexity autoencoder-based solution for CSI compression. By considering the task of CSI compression as an image compression problem, several works based on an autoencoder structure were proposed [13], [25], [38]–[43]. Notable works among them include CSINet [13], which was one of the first deep learning approaches proposed and outperformed compressed sensing baselines such as LASSO and BM3D-AMP. CRNet [25] proposed a multi-resolution deep learning framework for CSI feedback in massive MIMO systems, enabling scalable compression across different feedback overheads. Recently, a transformer-based architecture that utilizes stripe-wise spatial features was introduced in [44] to enhance the efficiency of CSI compression in massive MIMO systems.

A. Autoencoder-based CSI compression

Given the three-dimensional spatially correlated structure of the CSI matrix, using a convolution-based architecture is an efficient choice for compressing the input. We chose a low-complexity design for the auto-encoder. The encoder is implemented as lightweight CNN layers followed by a fully connected layer. To maintain robustness under changing signal-to-noise ratio (SNR) conditions, we use an SNR-adaptation module that dynamically scales the feature activations based on SNR. The complete architecture of both the encoder and the SNR-adaptation block is shown in Fig. 1.

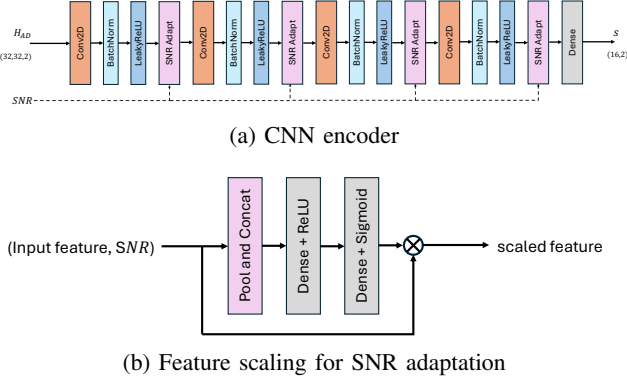


Fig. 1: Low-complexity CSI encoder.

The decoder employs a moderately deeper architecture to extract richer representations. It starts with a fully connected layer, followed by an initial convolutional layer and a stack of five residual blocks that enhance feature propagation and stabilize training. An identical SNR-adaptation module is employed in the decoder, mirroring the encoder design. A schematic of the decoder, including the residual block layout, is provided in Fig. 2.

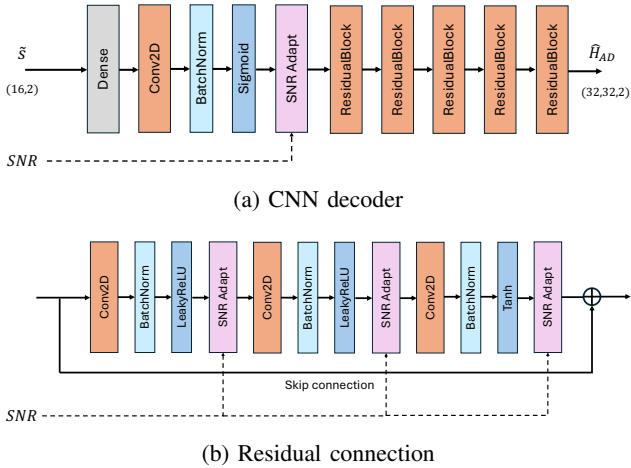


Fig. 2: Low-complexity CSI decoder.

We train the autoencoder in a supervised manner to learn an effective low-complexity compression scheme. The encoder compresses the continuous channel measurement H_d into a compact latent vector $s \in \mathbb{C}^k$. The decoder reconstructs

the approximate channel measurement \hat{H}_d . The encoder and decoder are jointly optimized in an end-to-end fashion to minimize the reconstruction loss for CSI. We use the MSE loss to enforce reconstruction fidelity by ensuring that the reconstructed output closely matches the input, given by:

$$\mathcal{L}_{\text{MSE}}(H_d, \hat{H}_d) = \|H_d - \hat{H}_d\|^2, \quad (2)$$

where $\|\cdot\|$ denotes the Frobenius norm.

Several works have demonstrated that CNN-based autoencoders can effectively minimize the reconstruction NMSE for both standalone CSI compression [13], [44] and joint source-channel coding of CSI [27]. Although this supervised formulation suffices for relatively simple channel distributions, it struggles when the underlying channel distribution becomes more complex. Recent work on CSI compression over the COST2100 outdoor channel [35] demonstrated that generative diffusion models significantly outperform conventional CNN autoencoders in such challenging settings. Motivated by these findings, we augment our autoencoder with a diffusion refinement stage at the base station. This hybrid design invokes the diffusion module only when the channel complexity warrants it, thereby delivering superior reconstruction quality without incurring unnecessary computational overhead in simpler channel conditions.

IV. RESIDUAL DIFFUSION FOR CSI ENHANCEMENT

In this section, we introduce a framework for enhancing CSI reconstruction at the receiver using residual diffusion [37]. Unlike conventional generative diffusion-based approaches, the proposed method can be seamlessly integrated with both learning-based and traditional non-learning-based techniques, as the diffusion module is trained as a standalone denoising model, making it more suitable for practical adaptation.

Preprocessing. To reduce computational complexity, we first transform the complex matrix H_d from the spatial-frequency domain to the angular-delay domain by applying a two-dimensional inverse fast Fourier transform (2D IFFT). This transformation exploits the inherent sparsity in the angular-delay domain, supported by established assumptions [45]. Subsequently, we retain only the first 32 elements along the delay dimension, as the remaining coefficients typically approach zero, yielding compact angular-delay domain representations of H_d . The original CSI matrices can be reconstructed by appending zero matrices of size $32 \times (N_c - 32)$ and performing a 2D FFT. This preprocessing procedure is widely recognized as an efficient CSI representation technique [13], [25], [46]. The performance evaluations reported in this work are conducted in terms of normalized mean squared error (NMSE), following the standard practice in CSI compression literature.

The receiver first obtains a coarse estimate of the channel using the autoencoder described in Sec. III-A, which we refer to as Stage 1. Unlike certain CSI compression methods that quantize the latent representation into a fixed number of bits using vector quantization, we instead map the latent to a fixed-length continuous vector. This continuous representation al-

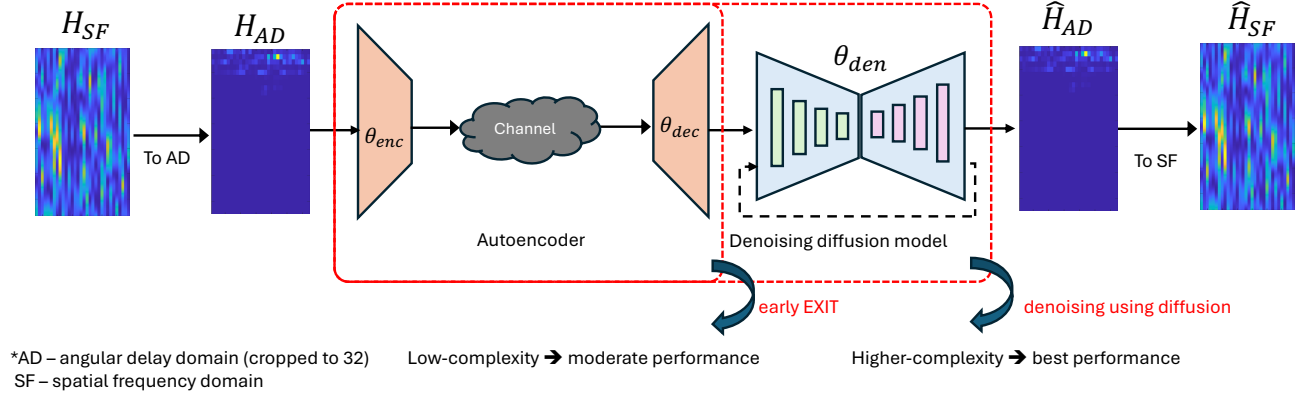


Fig. 3: A lightweight autoencoder compresses the MIMO CSI matrix into a low-dimensional latent representation, which is transmitted over a noisy channel. Decoding occurs in two stages: (1) a low-complexity decoder produces a coarse reconstruction, and (2) a diffusion-based denoising model refines the output for enhanced quality.

lows direct mapping of encoded data to the uplink subcarriers and simulates complex channel impairments such as multipath within the feedback channel.

In Stage 2, the denoising process leverages the output of the autoencoder to initialize the reverse diffusion procedure with the coarse CSI estimate. Following standard practice in the generative modeling literature, we adopt the U-Net architecture [47] as the backbone for the denoising network. Unlike recent generative diffusion-based CSI reconstruction methods [35], which initialize reverse diffusion from random Gaussian noise, we employ a residual diffusion approach that initializes the reverse diffusion with a coarse estimate provided by the autoencoder head and iteratively refines the CSI estimate, as illustrated in Fig. 3.

While initializing with random noise facilitates the generation of diverse samples from the underlying distribution—an objective well-suited for data synthesis—it is suboptimal for compression and reconstruction tasks, where compressed latent features already provide a strong prior. Residual diffusion addresses this by starting from a coarse channel estimate, leading to more accurate reconstructions. The effectiveness of residual diffusion for reconstruction tasks has been well demonstrated in the context of image compression [48]. We now formally describe the complete CSI compression and reconstruction pipeline.

In Stage 1, the encoder produces a compressed representation \mathbf{s} , which is then used to obtain a coarse reconstruction \hat{H}_d of the input channel H_d . During the denoising stage, the objective is to further refine \hat{H}_d by sampling $\mathbf{Z} \sim p(\mathbf{z} | \hat{H}_d)$. This leads to the formulation of a residual denoising diffusion process, given by

$$p(\mathbf{z}_{0:T} | \hat{H}_d) = p(\mathbf{z}_T) \prod_{t=1}^T \mathcal{N}(\mathbf{z}_{t-1}; \mu_\theta(\mathbf{z}_t, \hat{H}_d, t), \beta_t \mathbf{I}), \quad (3)$$

where $\mathbf{z}_{0:T} = (\mathbf{z}_0, \dots, \mathbf{z}_T)$ denotes a realization of the stochastic process $(\mathbf{Z}_0, \dots, \mathbf{Z}_T)$, μ_θ is the learnable mean function parameterized by θ , β_t defines the variance schedule at each time step t , and \mathbf{I} is the identity matrix.

In a generative diffusion-based approach, the forward process is defined by progressively adding Gaussian noise with variance $\beta_t \in (0, 1)$ to the clean latent features \mathbf{z}_0 according to a predefined schedule, as given by

$$\mathbf{z}_t = \sqrt{\bar{\alpha}_t} \mathbf{z}_0 + \sqrt{1 - \bar{\alpha}_t} \boldsymbol{\epsilon}_t, \quad t = 1, 2, \dots, T, \quad (4)$$

where $\boldsymbol{\epsilon}_t \sim \mathcal{N}(0, \mathbf{I})$, $\alpha_t = 1 - \beta_t$, and $\bar{\alpha}_t = \prod_{i=1}^t \alpha_i$. As t increases, the noisy latent variable \mathbf{z}_t gradually converges to a standard Gaussian distribution. Typically, T is chosen as a relatively large value (e.g., 20–50), with the reverse diffusion process initialized from pure Gaussian noise. However, in the context of CSI compression, this strategy is suboptimal, as a coarse channel estimate \hat{H}_d can be readily obtained using either conventional compression techniques [1] or low-complexity deep learning-based methods [49].

To exploit the availability of the coarse estimate \hat{H}_d , we adopt a residual diffusion approach as presented in [48], which modifies the initialization step as

$$\mathbf{z}_N = \sqrt{\bar{\alpha}_N} \hat{H}_d + \sqrt{1 - \bar{\alpha}_N} \boldsymbol{\epsilon}_N, \quad (5)$$

where $N \ll T$. This leads to the following residual diffusion formulation:

$$\mathbf{z}_t = \sqrt{\bar{\alpha}_t} (\mathbf{z}_0 + \eta_t \mathbf{r}) + \sqrt{1 - \bar{\alpha}_t} \boldsymbol{\epsilon}_t, \quad t = 1, 2, \dots, N, \quad (6)$$

where \mathbf{r} denotes the residual between the clean channel $\mathbf{z}_0 = H_d$ and the coarse estimate \hat{H}_d , i.e., $\mathbf{r} = \hat{H}_d - \mathbf{z}_0$. The weighting sequence $\{\eta_t\}_{t=1}^N$ is designed such that $\eta_1 \rightarrow 0$ and $\eta_N = 1$.

Since the residual \mathbf{r} is not available during inference, residual diffusion assumes a linear relationship among \mathbf{z}_{t-1} , \mathbf{z}_t , and \mathbf{z}_0 , analogous to the DDIM framework [29], given by

$$\mathbf{z}_{t-1} = k_t \mathbf{z}_0 + m_t \mathbf{z}_t + \sigma_t \boldsymbol{\epsilon}, \quad (7)$$

where $\sigma_t = 0$ for simplicity and k_t and m_t are weighing coefficients from [48]. Combining (6) and (7) yields

$$\frac{\eta_t}{\eta_{t-1}} = \frac{\sqrt{1 - \bar{\alpha}_t} / \sqrt{\alpha_t}}{\sqrt{1 - \bar{\alpha}_{t-1}} / \sqrt{\alpha_{t-1}}} \Rightarrow \eta_t = \lambda \frac{\sqrt{1 - \bar{\alpha}_t}}{\sqrt{\alpha_t}}, \quad (8)$$

where the scaling factor λ is set to $\frac{\sqrt{\bar{\alpha}_N}}{\sqrt{1-\bar{\alpha}_N}}$ to satisfy the condition $\eta_N = 1$.

Substituting (8) into (6), the forward diffusion process can be expressed as

$$\mathbf{z}_t = \sqrt{\bar{\alpha}_t} \left(\mathbf{z}_0 + \lambda \frac{\sqrt{1-\bar{\alpha}_t}}{\sqrt{\bar{\alpha}_t}} \mathbf{r} \right) + \sqrt{1-\bar{\alpha}_t} \boldsymbol{\epsilon}_t, \quad (9)$$

which simplifies to

$$\mathbf{z}_t = \sqrt{\bar{\alpha}_t} \mathbf{z}_0 + \sqrt{1-\bar{\alpha}_t} (\lambda \mathbf{r} + \boldsymbol{\epsilon}_t). \quad (10)$$

Ultimately, the denoising network is trained to recover the clean channel \mathbf{z}_0 from noisy observations at various noise levels encountered during the forward diffusion process. The corresponding diffusion loss is formulated as

$$\mathcal{L}_{\text{diff}} = \mathbb{E}_{\mathbf{z}_0, \mathbf{T}} \left[\frac{\bar{\alpha}_{\mathbf{T}}}{1-\bar{\alpha}_{\mathbf{T}}} \left\| \mathbf{z}_0 - f_{\text{den}}(\mathbf{z}_{\mathbf{T}}, \hat{H}_d, \mathbf{T}; \theta_{\text{den}}) \right\|^2 \right], \quad (11)$$

where $f_{\text{den}}(\cdot)$ is the denoising network parameterized by θ_{den} .

Diffusion with χ -prediction. In Equation (11), the loss is computed between the clean image and the model’s prediction, compelling the network to directly predict the image rather than the conventional approach of predicting the added noise. This technique, known as χ -prediction, proves particularly advantageous when operating with a limited number of denoising steps (e.g., $T < 50$). As our experimental results in subsequent sections demonstrate, this approach facilitates low-latency inference by enabling a transition to one-step decoding during inference with minimal or no degradation in reconstruction quality.

A. Training

We propose a two-stage training strategy to optimize performance while maintaining computational efficiency. In the first stage, the autoencoder model is trained using the MSE loss (2) between the input CSI matrix and the estimated CSI matrix. Due to the relatively small number of parameters and faster convergence, the computational overhead for Stage 1 is minimal. The detailed training procedure for this stage is outlined in Alg. 1.

Algorithm 1 Training the autoencoder model

Input: Initial model $(\theta_{\text{enc}}, \theta_{\text{dec}})$, Adam optimizer

Output: Updated model $(\theta_{\text{enc}}, \theta_{\text{dec}})$

- 1: **for** $i = 0$ to N_{train} **do**
 - 2: Sample H_d from the channel distribution
 - 3: $\mathbf{s} = f_{\text{enc}}(H_d; \theta_{\text{enc}})$
 - 4: $\hat{H}_d = f_{\text{dec}}(\mathbf{s}; \theta_{\text{dec}})$
 - 5: $\mathcal{L}_{\text{MSE}} = \|H_d - \hat{H}_d\|^2$
 - 6: Adam($\theta_{\text{enc}}, \theta_{\text{dec}}, \mathcal{L}_{\text{MSE}}$)
 - 7: **end for**
-

In the second stage, the weights of the autoencoder model are frozen, while a residual conditional denoising diffusion model, based on the U-Net architecture, is trained. This training process optimizes the diffusion loss defined in (11),

essentially training a denoising network. The detailed training procedure for this stage is outlined in Alg. 2.

Algorithm 2 Training the denoising U-Net

Input: Pretrained $(\theta_{\text{enc}}, \theta_{\text{dec}})$. Initial parameters for denoising network θ_{den} , variance schedule $\{\bar{\alpha}_t\}_{t=0}^T$, Adam optimizer

Output: Updated denoising network θ_{den}

- 1: **for** $i = 0$ to N_{train} **do**
 - 2: Sample H_d from the channel distribution
 - 3: $\mathbf{s} = f_{\text{enc}}(H_d; \theta_{\text{enc}})$
 - 4: $\hat{H}_d = f_{\text{dec}}(\mathbf{s}; \theta_{\text{dec}})$; $\mathbf{r} = \hat{H}_d - \mathbf{z}_0$
 - 5: $\mathcal{L}_{\text{diff}} = \frac{\bar{\alpha}_t}{1-\bar{\alpha}_t} \left\| \mathbf{z}_0 - f_{\text{den}}(\sqrt{\bar{\alpha}_t} \mathbf{z}_0 + \sqrt{1-\bar{\alpha}_t} (\lambda \mathbf{r} + \boldsymbol{\epsilon}_t)) \right\|^2$
 - 6: Adam($\theta_{\text{den}}, \mathcal{L}_{\text{diff}}$)
 - 7: **end for**
-

V. EXPERIMENTAL SETUP AND RESULTS

A. Baselines and comparison.

To evaluate our diffusion-based approach, we benchmark against ADJSCC [27], a recent state-of-the-art non-linear transform method. ADJSCC employs a neural network to transform CSI information from the spatial frequency domain to a low-dimensional representation—bypassing the traditional IFFT approach—before further compression via a secondary network. We also include the deep JSCC variant of CSINet+ [39], another widely recognized benchmark in CSI compression literature. To maintain fairness in comparison, we utilize identical datasets and training protocols across all evaluated models.

We implement two variants of the ADJSCC baseline: (1) the original architecture as presented in [27], and (2) a parameter-scaled version that matches the complexity of our proposed RD-JSCC model, by increasing the layers and channel dimensions. Additionally, we examine a supervised variant of RD-JSCC, where both the autoencoder and U-Net components are trained end-to-end using an MSE loss function. Our primary contribution, RD-JSCC—which integrates an autoencoder with diffusion-based U-Net training—demonstrates performance improvements of an order of magnitude compared to [27] at equivalent NMSE targets.

B. Dataset

We evaluate our method on the COST2100 outdoor dataset [50], which is widely adopted due to its realistic and complex channel characteristics. The dataset provides 10^5 training samples and 2×10^4 test samples. It is important to note that the original spatial-frequency domain representations are not publicly available; instead, we utilize the provided 32×32 cropped complex channel matrices in the angular-delay domain. Consequently, we omit the non-linear transformation module used in ADJSCC and retain only the inner encoder-decoder components that operate directly on the 32×32 angular-delay domain complex inputs. Since the input dimensions of the inner module match those of the COST2100 cropped channels, this setup enables a fair and consistent

comparison. All evaluations are reported in terms of NMSE measured in the angular-delay domain.

To simulate a realistic feedback channel, we generate uplink channel realizations using QuaDRiGa [36], adhering to the 3GPP TR 38.901 channel specification [51], with an uplink carrier frequency of 5.4 GHz. We adopt the simulation configuration outlined in [27] and assume line-of-sight (LOS). The base station (BS) is positioned at the center of a $20 \text{ m} \times 20 \text{ m}$ area and is equipped with a uniform linear array (ULA) comprising $N_t = 32$ omnidirectional elements spaced at half-wavelength intervals. The user equipment (UE) employs a single omnidirectional antenna ($N_r = 1$). The antenna heights are set to 3 m at the BS and 1.5 m at the UE. The simulation includes $N_c = 32$ subcarriers in the uplink transmission.

C. Model configuration

Encoder. To ensure a low-complexity design for the UE, we choose a small number of convolution channels and do not utilize any residual connections in the encoder architecture. The detailed architectural choices are summarized in Tab. I.

Layer	Channels	Kernel size
Input Conv	2	(11,11)
Conv layer 1	32	(9,9)
Conv layer 2	48	(7,7)
Output Conv	2	(5,5)

TABLE I: CNN encoder.

Decoder. The receiver employs a series of residual blocks with varying channel widths and kernel sizes. This deeper architecture, combined with residual connections, enhances reconstruction performance while introducing only a modest increase in decoding latency. The detailed architectural choices are summarized in Tab. II.

Layer	Channels	Kernel size
Input Conv	2	(7,7)
Residual Block Conv layer 1	16	(7,7)
Residual Block Conv layer 2	24	(5,5)
Residual Block Conv layer 3	2	(3,3)

TABLE II: Residual Block decoder.

Diffusion. The architecture for the diffusion denoising network is based on [30] and [35]. We choose an initial embedding width of 64 channels and dimension multipliers $\{1, 2, 3, 4\}$ for the successive down-sampling and mirrored up-sampling stages. Skip connections link each down-sampling block to its symmetric up-sampling counterpart, preserving high-resolution features throughout the reverse diffusion trajectory. The U-Net outputs a refined estimate of the CSI matrix that is fed back, iteratively refining the coarse estimate, based on the number of steps used in reverse diffusion.

D. Hyperparameters for training

To train the diffusion model, we adopt a similar training methodology and set of hyperparameters used in [35]. The

Adam optimizer is employed with a cosine annealing learning rate scheduler that goes from an initial learning rate of 3×10^{-4} to 1×10^{-5} , and a batch size of 100 is used. For the diffusion process, we use a cosine beta schedule for determining the noise variance at each step.

As described in Sec. IV, the model is trained in two stages. In the first stage, the autoencoder model is trained for $N_{\text{train}} = 10^5$ iterations using the MSE loss (2). In the second stage, the diffusion-based U-Net is trained for $N_{\text{train}} = 10^6$ iterations. The coarse estimate produced by the autoencoder serves as the initialization point for reverse diffusion, with denoising performed over $T = 20$ steps during training. However, during inference, we can use a 2-step denoising for the reverse diffusion, with a small penalty in performance. This is primarily enabled by training the diffusion model using *x-prediction* instead of Gaussian noise, thus making the inference $10 \times$ faster. Performance is evaluated using the NMSE, which is given as $\mathbb{E}[\|\mathbf{z} - \hat{\mathbf{z}}\|/\|\mathbf{z}\|]$ for the ground truth \mathbf{z} and reconstruction $\hat{\mathbf{z}}$.

E. Results

In Fig. 4, we present the NMSE in reconstruction for the angular-delay domain CSI measurements of the COST2100 outdoor dataset. We configured the feedback bandwidth to $k = 16$, compressing each 32×32 CSI measurement (1024 complex coefficients) to a 16-dimensional complex latent vector, achieving a compression rate of $1/64$. Note that for the COST2100 outdoor dataset, the NMSE reported is in the cropped angular-delay domain.

Our evaluation begins with the exact architectures from ADJSCC [27] and CSINet+ [39], which demonstrate notably poor performance. When scaling these architectures by incorporating additional intermediate layers and increasing convolutional channels, performance improves marginally, but all schemes still saturate at an NMSE greater than -4 dB. This reveals that conventional autoencoder approaches trained with supervised learning objectives exhibit poor scaling characteristics relative to model size and fail to adequately capture the underlying channel characteristics despite substantial parameter counts.

We then developed a hybrid architecture combining the original autoencoder model from [27] with a U-Net backbone for denoising. The U-Net backbone has been widely employed in image processing for enhanced denoising, deblurring, and, more recently, image generation. Our hybrid model, termed U-Net based JSCC, was trained with the same supervised training objective as [27], minimizing the end-to-end MSE. Remarkably, despite having a similar parameter count as the larger variants of ADJSCC and CSINet+, the U-Net-based JSCC shows significant performance improvements, achieving an NMSE lower than -9 dB. This highlights the importance of architectures that scale effectively with increasing model size.

Finally, we trained the U-Net-based JSCC model with a diffusion objective instead of the supervised objective. This approach, which we refer to as RD-JSCC, achieves the best performance among all evaluated schemes. During decoding

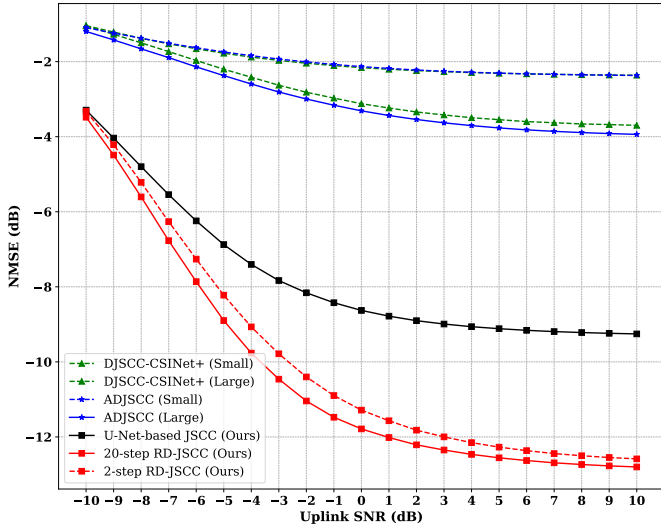


Fig. 4: RD-JSCC achieves an order-of-magnitude improvement in performance over state-of-the-art deep JSCC baselines on the COST2100 outdoor dataset for feedback bandwidth of $k = 16$.

at the receiver, the autoencoder head first produces a coarse estimate of the CSI. The U-Net model then initializes the reverse diffusion with this coarse estimate and refines the CSI at each denoising step, iteratively feeding the improved estimate back into the U-Net until completing the specified number of denoising steps. While our default configuration uses 20 denoising steps, we found that to minimize inference latency, a 2-step reverse diffusion performs remarkably well with only a negligible NMSE penalty, achieving an NMSE below -12 dB.

Remark 1. Diffusion-based modeling demonstrates a clear advantage in capturing complex channel distributions, particularly when conventional supervised methods struggle to represent such distributions effectively.

F. NMSE Performance Translation to BLER

While NMSE is the widely adopted metric for reporting CSI compression performance, block error rate (BLER) provides a more direct measure of practical system reliability. We therefore evaluate the uncoded BLER performance to assess how NMSE improvements translate to error rate reductions. For the COST2100 dataset, we construct SF domain data from the available AD domain measurements using fast Fourier transform (FFT), assuming lossless SF to AD transformation in the original dataset. As shown in Fig. 5, both methods achieve similar BLER performance at low SNR values. However, in the high-SNR regime, the U-Net based approach saturates around 10^{-4} BLER, while the diffusion-based RD-JSCC continues improving and reaches $\text{BLER} \approx 10^{-6}$ at 5 dB uplink SNR. This performance difference correlates with the underlying reconstruction quality: U-Net based JSCC achieves $\text{NMSE} \approx -9.2$ dB while RD-JSCC achieves $\text{NMSE} \approx -12.2$ dB, at a SNR of 5 dB in the uplink.

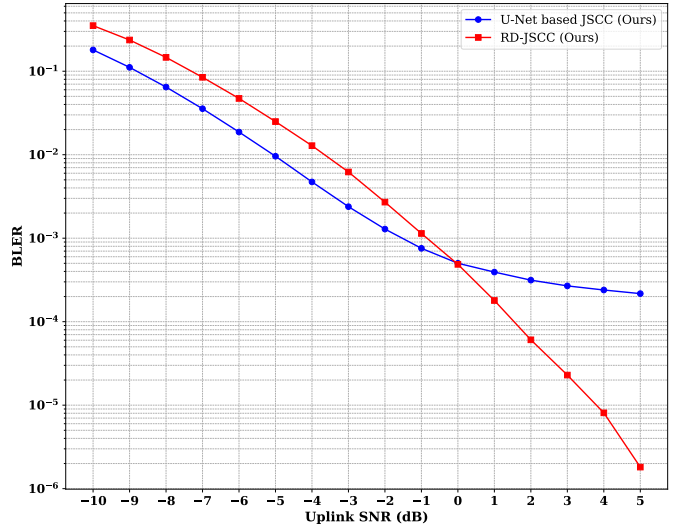


Fig. 5: Uncoded BLER performance comparison between U-Net based JSCC and RD-JSCC approaches. The diffusion-based method shows continued improvement at high SNR, achieving $\text{BLER} \approx 10^{-6}$ at 5 dB while the U-Net approach saturates around 10^{-4} .

Remark 2. For the COST2100-outdoor dataset, at a uplink SNR of 5 dB, the 3 dB improvement in NMSE of the CSI translates to approximately two orders of magnitude improvement in BLER, demonstrating that the NMSE gains from diffusion-based approach translates to reduced error floor in high-SNR conditions for improved reliability.

G. Computational Complexity

We now evaluate the computational complexity of RD-JSCC by measuring the throughput of each module on both the COST2100 outdoor and 3GPP indoor datasets. Throughput is measured in terms of samples processed per second (samples/s), averaged over multiple runs with a batch size of 10^3 . All simulations were conducted on a system equipped with an AMD Ryzen Threadripper PRO 5975WX 32-Core processor and an NVIDIA GeForce RTX 4090 GPU.

As shown in Tables III and IV, the encoder and decoder exhibit high throughput due to their lightweight convolutional architecture. The encoder consistently achieves throughput near 9.5×10^4 samples/s across both datasets, making it suitable for low-power UEs. The decoder is slightly more complex due to residual layers, but still maintains a high throughput of approximately 8.25×10^4 samples/s.

In contrast, the diffusion model, though delivering significant performance improvements under complex channel conditions, introduces a higher computational cost. The 2-step residual diffusion refinement achieves throughput of 3.9×10^3 samples/s on COST2100 and 8.2×10^3 samples/s on the 3GPP indoor dataset. For applications requiring higher fidelity, the full 20-step diffusion yields throughput in the 10^2 samples/s range, although the improvements in NMSE are marginal compared to 2-step diffusion. Hence, invoking the diffusion re-

Module	Throughput (samples/s)
Encoder	9.5×10^4
Decoder	8.2×10^4
Diffusion (2-step)	3.9×10^3
Diffusion (20-step)	3.9×10^2

TABLE III: Throughput of modules in RD-JSCC for COST2100.

Module	Throughput (samples/s)
Encoder	9.5×10^4
Decoder	8.2×10^4
Diffusion (2-step)	8.5×10^3
Diffusion (20-step)	8.5×10^2

TABLE IV: Throughput of modules in RD-JSCC for 3GPP indoor.

finement module at the decoder can incur a throughput penalty of $10\times$ to $100\times$, and should therefore be used judiciously, only when necessary, based on the underlying channel complexity.

These results reinforce the practicality of RD-JSCC’s hybrid decoding strategy, unlike a single diffusion-based solution presented in [35]. For simple channels, the decoder alone may suffice, while complex scenarios can selectively invoke diffusion-based refinement. Furthermore, early-exit and low-step inference modes offer flexible complexity-performance trade-offs.

VI. VARIABLE RATE COMPRESSION

In practical wireless communication systems, the available uplink bandwidth for CSI feedback varies dynamically due to factors such as performance requirements and network congestion. Traditionally, deep learning-based compression methods address multiple compression rates by training separate models for each rate. However, this approach imposes significant overhead on resource-constrained user equipment (UE). To mitigate this, recent research has focused on developing single-model solutions capable of handling multiple compression rates.

For instance, CSI-PPNet [52] introduces a one-sided architecture that supports arbitrary compression ratios using a single deep learning model. This design significantly reduces the number of parameters required at the UE, enhancing efficiency and simplifying deployment. Similarly, the Variable-Rate Code (VRC) approach dynamically allocates feedback bits based on estimated distortion, optimizing the trade-off between compression rate and reconstruction quality [26].

A. Matryoshka Representation Learning

Matryoshka Representation Learning (MRL), introduced in [53], is a representation learning framework designed to support multiple compression rates within a single model. The key idea behind MRL is to learn a single hierarchical representation that can be truncated at different lengths to yield compressed representations of varying fidelity. This is achieved by partitioning the learned representation vector into nested subsets, such that each prefix subset corresponds to a progressively higher compression rate. Importantly, MRL

enforces joint optimization of all nested representations during training, enabling the model to perform well across a broad spectrum of rate-distortion trade-offs without the need for retraining or maintaining multiple models. This design allows for efficient and adaptive deployment in scenarios with dynamic bandwidth or storage constraints, while maintaining representational consistency and strong generalization across different rates.

To enable CSI feedback compression at multiple target bandwidths $\{k_1, k_2, \dots, k_m\}$, the standard reconstruction loss (2) is extended to account for the cumulative reconstruction errors at each compression level. Specifically, the loss function is modified as

$$\mathcal{L}_{\text{MRL}} = \sum_{i=1}^m \lambda_i \|H_d - \hat{H}_d^{(k_i)}\|^2, \quad (12)$$

where $\hat{H}_d^{(k_i)}$ denotes the reconstructed CSI from the compressed representation of dimension k_i , and λ_i are weighting factors that balance the importance across different rates. We choose $\lambda_i = 1$ by default, assigning equal importance to all rates.

In Fig. 6, we show the results for the model optimized for 3 different feedback bandwidths $k = \{8, 16, 32\}$. We begin by choosing an encoder architecture to compress to a complex-valued latent dimension of 32 and mask the appropriate elements using the MRL objective to create latents of dimensions of size 16 and 8. Based on available bandwidth, the encoder automatically chooses the best possible latent dimension, achieving an efficient rate-distortion trade-off across a range of feedback rates. We note that at a feedback bandwidth of $k = 16$, we observe superior performance in Fig. 6 compared to Fig. 4. This improvement comes from the enhanced encoder complexity in terms of larger *Dense layer* required to accommodate the higher feedback bandwidth of $k = 32$, which consequently benefits performance across all bandwidth configurations.

VII. PRACTICAL CONSIDERATIONS

A. Channel Distribution vs. Model Complexity

While it is clear that diffusion models have the potential to enhance CSI reconstruction quality at the base station significantly, they also introduce substantial computational complexity. Therefore, it is crucial to justify this added complexity by employing diffusion-based refinement only when truly necessary. In the current state-of-the-art diffusion-based CSI compression method [35], the same network architecture is applied across both the Clustered Delay Line (CDL) and the more challenging COST2100 outdoor datasets, despite the latter being considerably more complex. Moreover, the comparisons to existing baselines do not account for the substantial differences in model size. For example, baseline models used in [35] such as CSINet and CRNet typically have around 400K parameters, whereas the generative diffusion-based approach presented utilizes approximately 15M parameters. This significant disparity in parameter count complicates

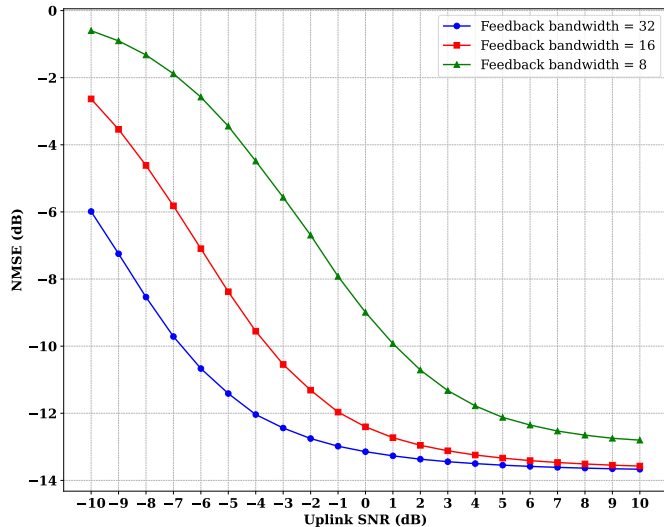


Fig. 6: Optimizing for multiple feedback bandwidths using a single model with MRL objective. RD-JSCC dynamically adapts the latent dimensionality based on the available uplink bandwidth, achieving an efficient rate-distortion trade-off across a range of feedback rates.

the assessment of whether performance gains arise from the diffusion modeling itself or simply from increased model size.

In this section, we conduct a systematic ablation study to isolate the benefits of diffusion modeling and to understand its advantages relative to the underlying channel complexity.

Architecture Choices. We evaluate three different architectures for this study. First, we consider a simple convolutional autoencoder trained in a supervised manner. Second, we consider an autoencoder followed by a U-Net denoising network, also trained end-to-end with supervised loss. Finally, we evaluate the RD-JSCC model, where the autoencoder and U-Net are trained jointly using the residual diffusion objective. In all three cases, the architectures are appropriately scaled to maintain comparable parameter counts across models. Complete details of parameters used in each experiment are provided below, in Tab. V and Tab. VI.

Channel Model Choices. In addition to the COST2100 outdoor scenario [50] analyzed in Sec. V, we now evaluate performance under the indoor open-area channel model specified in 3GPP TR 38.901 [51]. This environment is characterized by significantly lower spatial complexity and information density than COST2100, providing a useful contrast in dataset complexity. As seen in Sec. V, we first convert the spatial-frequency data into cropped angular-delay domain, preserving the first 32 subcarriers. But, after decompression, we convert the estimated channel matrices from the cropped angular-delay domain back to the spatial-frequency domain and subsequently present the final NMSE results in the original SF domain.

Analysis of results in Fig. 7 reveals that the performance gap between our diffusion-based approach and autoencoder baselines narrows considerably for the 3GPP indoor dataset, in stark contrast to the COST2100 outdoor results presented in Fig. 4. This observation highlights an important nuance:

Model	Encoder	Decoder	Denoising Model
DJSCC-CSINet+ (Small)	152K	118K	–
DJSCC-CSINet+ (Large)	152K	12M	–
ADJSCC (Small)	152K	118K	–
ADJSCC (Large)	152K	12M	–
U-Net-based JSCC	152K	118K	13.7M
RD-JSCC	152K	118K	13.9M

TABLE V: Parameter count for each model architecture used for COST2100 dataset experiment.

Model	Encoder	Decoder	Denoising Model
DJSCC-CSINet+ (Small)	167K	191K	–
DJSCC-CSINet+ (Large)	167K	1.3M	–
ADJSCC (Small)	168K	197K	–
ADJSCC (Large)	168K	1.3M	–
U-Net-based JSCC	152K	118K	1.25M
RD-JSCC	152K	118K	1.28M

TABLE VI: Parameter count for each model architecture used for 3GPP indoor dataset experiment.

Remark 3. Despite the general superiority of diffusion-based CSI compression, the complexity-performance trade-off becomes less favorable when modeling simpler channel environments, where conventional low-complexity autoencoder architectures may offer a more efficient solution.

Notably, the flexible formulation of our residual diffusion framework provides an additional operational advantage, allowing for early termination of the decoding process after stage 1, regardless of prevailing channel conditions, thereby offering adaptive decoding complexity scaling depending on application requirements.

B. Imperfect Channel Estimation

In the CSI compression literature, it is common to assume perfect CSI at UE. While this assumption is convenient for algorithm development and benchmarking, it rarely holds true in practical wireless communication systems. In realistic deployments, CSI must be acquired through pilot-based estimation at the receiver, which introduces errors due to noise, interference, and limited pilot resources. These estimation inaccuracies can significantly degrade the performance of both traditional and learning-based CSI compression schemes.

To bridge this gap, we explicitly incorporate channel estimation errors into our problem formulation. Specifically, we model the estimated downlink channel \tilde{H}_d as

$$\tilde{H}_d = H_d + E, \quad (13)$$

where $H_d \in \mathbb{C}^{N_c \times N_t}$ is the true downlink channel matrix, and $E \in \mathbb{C}^{N_c \times N_t}$ represents the estimation error. Each entry of E is modeled as a zero-mean complex Gaussian random variable, with variance determined by the channel-to-noise ratio (CNR). This additive error model is commonly used to model the uncertainty inherent in practical CSI acquisition [27].

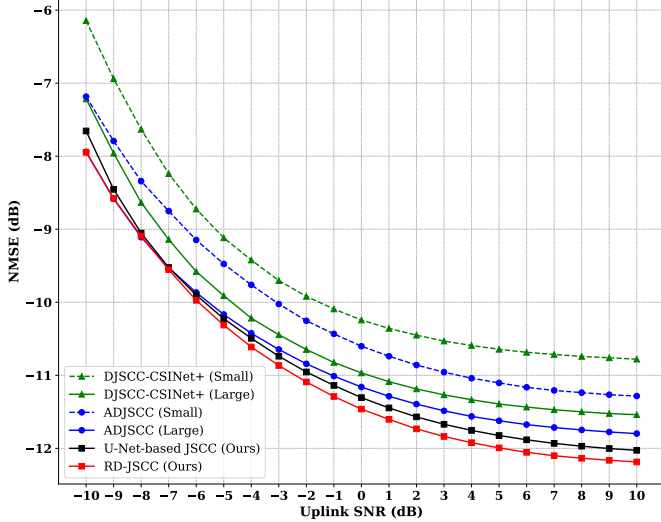


Fig. 7: Under low-complexity channel conditions, such as the 3GPP indoor scenario, the performance gap between diffusion-based and autoencoder-based approaches narrows significantly.

In Fig. 8, we observe that RD-JSCC trained under the perfect CSI assumption suffers a substantial performance drop when exposed to severe channel estimation errors, particularly at a CNR of 0 dB. However, by incorporating channel estimation error directly into the training pipeline, RD-JSCC learns to operate robustly under imperfect CSI conditions, recovering most of the performance degradation.

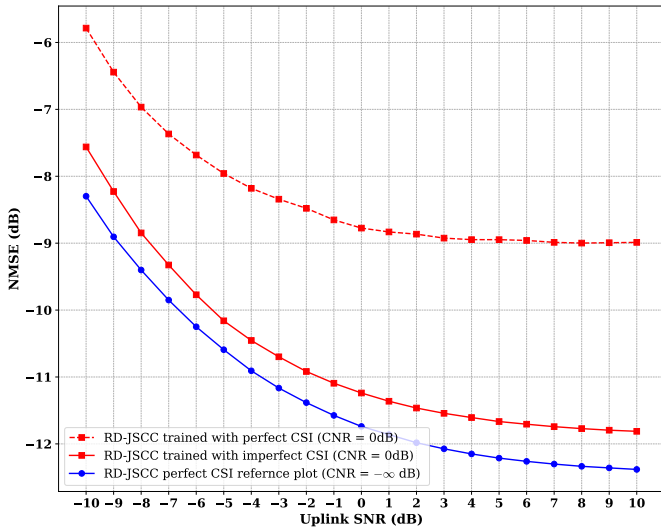


Fig. 8: By injecting channel estimation errors into the training pipeline, RD-JSCC becomes robust to imperfect CSI and recovers much of the performance degradation caused by estimation noise when tested at a CNR of 0 dB.

C. Effect of Quantization

When using autoencoders for data compression, the encoder typically produces a continuous latent vector $\mathbf{s} \in \mathbb{C}^k$, which is often stored using 32-bit floating-point precision. This imposes

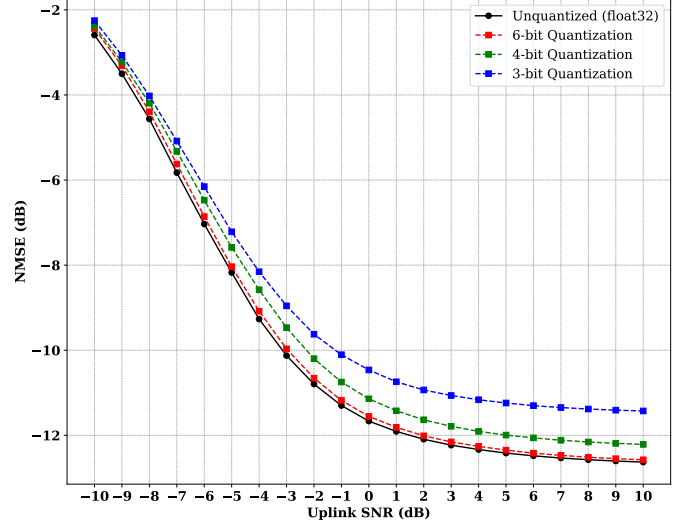


Fig. 9: Effect of fixed-bit quantization on reconstruction quality. The encoder output can be quantized to as low as 4 bits per dimension with negligible degradation in reconstruction performance.

a significant memory and communication overhead, especially in resource-constrained scenarios such as edge devices or embedded wireless systems. To reduce this burden, we utilize a companding-based quantization scheme that enables fixed-bit representation of latent vectors with minimal degradation in reconstruction performance. Note that we quantize the real and imaginary values independently, using identical techniques.

Specifically, we first apply μ -law companding to the latent vector to non-linearly compress its dynamic range, using the transformation:

$$s'_i = \text{sign}(s_i) \cdot \frac{\log(1 + \mu|s_i|)}{\log(1 + \mu)},$$

where μ is a positive scalar hyperparameter (set to $\mu = 50$ in our experiments). This transformation increases the quantization resolution near zero, where the latent values are often concentrated. The companded latent s' is then passed through a uniform scalar quantizer with B bits per dimension. During training, this quantization is implemented with a straight-through estimator to enable end-to-end gradient flow.

At inference, the quantized codes are dequantized and passed through the inverse μ -law transformation:

$$\hat{s}_i = \text{sign}(s'_i) \cdot \frac{(1 + \mu)^{|s'_i|} - 1}{\mu},$$

which approximately reconstructs the original latent vector. As shown in Fig. 9, this scheme enables us to quantize the latent space down to $B = 4$ bits per dimension with negligible performance loss, offering a practical and efficient solution for deployment in memory and bandwidth-limited systems.

VIII. ABLATION

A. Contribution of Residual Diffusion Formulation

To quantify the impact of the residual formulation in our denoising diffusion process, we conduct an ablation study

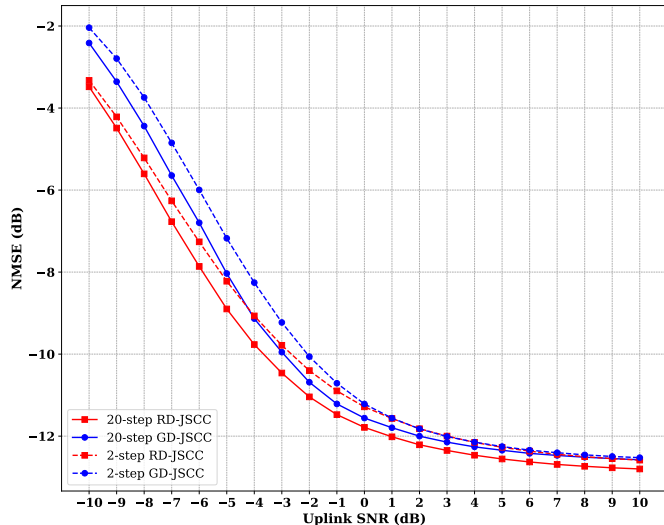


Fig. 10: Comparison between standard GD-JSCC and our proposed RD-JSCC for feedback bandwidth $k = 16$. By initializing reverse diffusion with a coarse CSI estimate and modifying the denoising objective to predict residual noise, RD-JSCC achieves up to 1 dB SNR improvement for a target NMSE.

comparing our proposed RD-JSCC scheme against a conventional GD-JSCC baseline. The baseline follows the standard formulation introduced in [35], where the reverse diffusion process is initialized from pure Gaussian noise and trained to generate the CSI purely based on the conditioning signal. In contrast, RD-JSCC initializes the reverse diffusion with a coarse reconstruction obtained from a lightweight autoencoder and performs iterative denoising on the residual between the ground-truth CSI and this initial estimate.

This residual formulation enables a modified diffusion objective that focuses on learning the residual signal, which is often sparser and easier to model. As shown in Fig. 10, RD-JSCC consistently outperforms the GD-JSCC baseline across all tested SNR levels. Notably, it achieves up to a 1 dB improvement in effective SNR for a target NMSE, clearly demonstrating the advantages of the residual formulation in diffusion-based compression.

B. Contribution of Encoder

To investigate the role of encoder complexity in our architecture, we conducted ablation studies varying the encoder depth and channel capacity. Despite comprising a relatively small fraction of the overall model parameters, Fig. 11 demonstrates that encoder design significantly impacts reconstruction quality. When reducing our standard 4-layer encoder to a lighter 2-layer variant with fewer channels, performance deteriorates substantially—up to 2 dB loss in NMSE at equivalent compression rates. This confirms that the encoder, while computationally efficient, serves a critical function in extracting and preserving essential features from the input signal. These preserved features subsequently enable both the decoder and diffusion modules to achieve high-quality reconstruction.

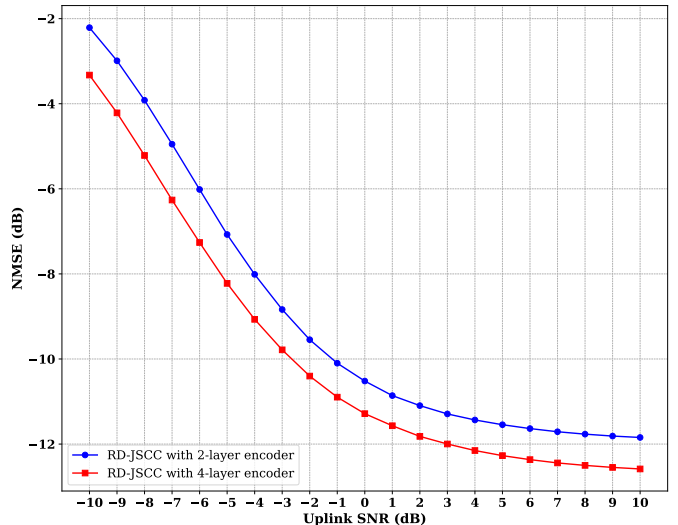


Fig. 11: Impact of encoder complexity on reconstruction performance. Reducing from a 4-layer to a 2-layer architecture with fewer channels degrades NMSE by up to 2 dB on the COST2100 dataset at a feedback bandwidth of $k = 16$, despite the encoder’s minimal contribution to overall model complexity.

The exact architecture choices for the 2-layer and 4-layer encoder are provided in Tab. VII. The 2-layer encoder has a total of 66K parameters, and the 4-layer encoder has a total of 152K parameters. For reference, we recall from Tab. V that the full RD-JSCC model has $\approx 14\text{M}$ parameters. Our findings suggest that appropriate encoder complexity represents an important design consideration that disproportionately influences overall system performance relative to its parameter count.

Layer	4-Layer Encoder		2-Layer Encoder	
	Channels	Kernel size	Channels	Kernel size
Input Conv	2	(11,11)	2	(7,7)
Conv layer 1	32	(9,9)	2	(7,7)
Conv layer 2	48	(7,7)	–	–
Output Conv	2	(5,5)	–	–

TABLE VII: Comparison between 4-layer encoder and lightweight 2-layer encoder architectures used in ablation studies. The 4-layer configuration provides superior feature extraction capabilities, leading to better reconstruction performance as demonstrated in Fig. 11.

IX. CONCLUSION AND REMARKS

In this work, we introduce a hybrid JSCC scheme for MIMO CSI compression combining autoencoder-based initial estimation with diffusion-based refinement. Our residual diffusion approach initializes reverse diffusion with a coarse autoencoder estimate, tailoring the reverse diffusion specifically for reconstruction. This two-stage framework can be exited after either stage based on channel conditions and performance requirements, balancing computational complexity against fidelity. Further, using χ -prediction, we enable single-step diffusion inference with minimal performance loss, substantially reducing latency. Our experiments across varying

channel complexities show diffusion-based refinement delivers optimal value for complex channel distributions, while auto-encoder solutions efficiently serve simpler channel distributions. These findings highlight diffusion models' potential for enhancing CSI reconstruction at base stations under challenging uplink conditions. Future work includes developing multi-rate compression within a single model, investigating quantization effects, exploring weight quantization techniques, and optimizing the U-Net backbone for improved computational efficiency while preserving performance. Further, including additional loss terms such as the binary cross entropy loss between transmitted and received data or the effective MIMO channel capacity, to directly optimize for the downstream task [19] is also an interesting direction.

REFERENCES

- [1] M. S. Sim, J. Park, C.-B. Chae, and R. W. Heath, "Compressed channel feedback for correlated massive MIMO systems," *Journal of Communications and Networks*, vol. 18, no. 1, pp. 95–104, 2016.
- [2] H. Kim, Y. Jiang, R. Rana, S. Kannan, S. Oh, and P. Viswanath, "Communication algorithms via deep learning," *arXiv preprint arXiv:1805.09317*, 2018.
- [3] A. V. Makkuva, X. Liu, M. V. Jamali, H. Mahdaviifar, S. Oh, and P. Viswanath, "Ko codes: inventing nonlinear encoding and decoding for reliable wireless communication via deep-learning," in *International Conference on Machine Learning*. PMLR, 2021, pp. 7368–7378.
- [4] M. V. Jamali, H. Saber, H. Hatami, and J. H. Bae, "Productae: Toward training larger channel codes based on neural product codes," in *ICC 2022-IEEE International Conference on Communications*. IEEE, 2022, pp. 3898–3903.
- [5] S. K. Ankireddy, S. A. Hebbbar, H. Wan, J. Cho, and C. Zhang, "Nested construction of polar codes via transformers," in *2024 IEEE International Symposium on Information Theory (ISIT)*. IEEE, 2024, pp. 1409–1414.
- [6] S. K. Ankireddy, K. Narayanan, and H. Kim, "LightCode: Light analytical and neural codes for channels with feedback," *IEEE Journal on Selected Areas in Communications*, 2025.
- [7] E. Nachmani, Y. Be'ery, and D. Burshtein, "Learning to decode linear codes using deep learning," in *2016 54th Annual Allerton Conference on Communication, Control, and Computing (Allerton)*. IEEE, 2016, pp. 341–346.
- [8] N. Shlezinger, N. Farsad, Y. C. Eldar, and A. J. Goldsmith, "ViterbiNet: A deep learning based Viterbi algorithm for symbol detection," *IEEE Transactions on Wireless Communications*, vol. 19, no. 5, pp. 3319–3331, 2020.
- [9] Y. Choukroun and L. Wolf, "Error correction code transformer," *Advances in Neural Information Processing Systems*, vol. 35, pp. 38 695–38 705, 2022.
- [10] S. A. Hebbbar, R. K. Mishra, S. K. Ankireddy, A. V. Makkuva, H. Kim, and P. Viswanath, "TinyTurbo: Efficient Turbo Decoders on Edge," in *2022 IEEE International Symposium on Information Theory (ISIT)*. IEEE, 2022, pp. 2797–2802.
- [11] S. K. Ankireddy and H. Kim, "Interpreting Neural Min-Sum Decoders," in *ICC 2023-IEEE International Conference on Communications*. IEEE, 2023, pp. 6645–6651.
- [12] S. A. Hebbbar, S. K. Ankireddy, H. Kim, S. Oh, and P. Viswanath, "DeepPolar: Inventing Nonlinear Large-Kernel Polar Codes via Deep Learning," *arXiv preprint arXiv:2402.08864*, 2024.
- [13] C.-K. Wen, W.-T. Shih, and S. Jin, "Deep learning for massive MIMO CSI feedback," *IEEE Wireless Communications Letters*, vol. 7, no. 5, pp. 748–751, 2018.
- [14] C.-J. Chun, J.-M. Kang, and I.-M. Kim, "Deep learning-based channel estimation for massive MIMO systems," *IEEE Wireless Communications Letters*, vol. 8, no. 4, pp. 1228–1231, 2019.
- [15] M. Soltani, V. Pourahmadi, A. Mirzaei, and H. Sheikhzadeh, "Deep learning-based channel estimation," *IEEE Communications Letters*, vol. 23, no. 4, pp. 652–655, 2019.
- [16] P.-H. Kuo, H. Kung, and P.-A. Ting, "Compressive sensing based channel feedback protocols for spatially-correlated massive antenna arrays," in *2012 IEEE Wireless Communications and Networking Conference (WCNC)*. IEEE, 2012, pp. 492–497.
- [17] J. Ballé, V. Laparra, and E. P. Simoncelli, "End-to-end optimized image compression," *arXiv preprint arXiv:1611.01704*, 2016.
- [18] J. Ballé, D. Minnen, S. Singh, S. J. Hwang, and N. Johnston, "Variational image compression with a scale hyperprior," *arXiv preprint arXiv:1802.01436*, 2018.
- [19] P.-h. Li, S. K. Ankireddy, R. P. Zhao, H. Nourkhiz Mahjoub, E. Moradi Pari, U. Topcu, S. Chinchali, and H. Kim, "Task-aware distributed source coding under dynamic bandwidth," *Advances in Neural Information Processing Systems*, vol. 36, pp. 406–417, 2023.
- [20] J. Li, B. Li, and Y. Lu, "Neural video compression with diverse contexts," in *Proceedings of the IEEE/CVF conference on computer vision and pattern recognition*, 2023, pp. 22 616–22 626.
- [21] J. Guo, C.-K. Wen, S. Jin, and G. Y. Li, "Overview of deep learning-based CSI feedback in massive MIMO systems," *IEEE Transactions on Communications*, vol. 70, no. 12, pp. 8017–8045, 2022.
- [22] T. Wang, C.-K. Wen, S. Jin, and G. Y. Li, "Deep Learning-Based CSI Feedback Approach for Time-Varying Massive MIMO Channels," *IEEE Wireless Communications Letters*, vol. 8, no. 2, pp. 416–419, 2019. [Online]. Available: <https://ieeexplore.ieee.org/document/8576629>
- [23] Q. Li, A. Zhang, P. Liu, J. Li, and C. Li, "A Novel CSI Feedback Approach for Massive MIMO Using LSTM-Attention CNN," *IEEE Access*, vol. 8, pp. 7295–7302, 2020. [Online]. Available: <https://ieeexplore.ieee.org/document/8949444>
- [24] Y. Liu and O. Simeone, "HyperRNN: Deep Learning-Aided Downlink CSI Acquisition via Partial Channel Reciprocity for FDD Massive MIMO," in *2021 IEEE 22nd International Workshop on Signal Processing Advances in Wireless Communications (SPAWC)*, 2021, pp. 31–35. [Online]. Available: <https://ieeexplore.ieee.org/document/9593122>
- [25] Z. Lu, J. Wang, and J. Song, "Multi-resolution CSI feedback with deep learning in massive MIMO system," in *ICC 2020-2020 IEEE international conference on communications (ICC)*. IEEE, 2020, pp. 1–6.
- [26] H. Kim, H. Kim, and G. de Veciana, "Learning variable-rate codes for CSI feedback," in *Proceedings of the IEEE Global Communications Conference (GLOBECOM)*, 2022, pp. 1435–1441.
- [27] J. Xu, B. Ai, N. Wang, and W. Chen, "Deep joint source-channel coding for csi feedback: An end-to-end approach," *IEEE Journal on Selected Areas in Communications*, vol. 41, no. 1, pp. 260–273, 2022.
- [28] J. Ho, A. Jain, and P. Abbeel, "Denoising diffusion probabilistic models," *Advances in neural information processing systems*, vol. 33, pp. 6840–6851, 2020.
- [29] J. Song, C. Meng, and S. Ermon, "Denoising diffusion implicit models," *arXiv preprint arXiv:2010.02502*, 2020.
- [30] R. Yang and S. Mandt, "Lossy image compression with conditional diffusion models," *Advances in Neural Information Processing Systems*, vol. 36, pp. 64 971–64 995, 2023.
- [31] M. Careil, M. J. Muckley, J. Verbeek, and S. Lathuilière, "Towards image compression with perfect realism at ultra-low bitrates," in *The Twelfth International Conference on Learning Representations*, 2023.
- [32] Q. Mao, T. Yang, Y. Zhang, Z. Wang, M. Wang, S. Wang, L. Jin, and S. Ma, "Extreme image compression using fine-tuned vqgans," in *2024 Data Compression Conference (DCC)*. IEEE, 2024, pp. 203–212.
- [33] A. Li, F. Li, Y. Liu, R. Cong, Y. Zhao, and H. Bai, "Once-for-All: Controllable Generative Image Compression with Dynamic Granularity Adaption," *arXiv preprint arXiv:2406.00758*, 2024.
- [34] T. Celik, "Spatial entropy-based global and local image contrast enhancement," *IEEE Transactions on Image Processing*, vol. 23, no. 12, pp. 5298–5308, 2014.
- [35] H. Kim, T. Lee, H. Kim, G. De Veciana, M. A. Arfaoui, A. Koc, P. Pietraski, G. Zhang, and J. Kaewell, "Generative Diffusion Model-based Compression of MIMO CSI," *arXiv preprint arXiv:2503.03753*, 2025.
- [36] S. Jaeckel, L. Raschkowski, K. Börner, L. Thiele, F. Burkhardt, and E. Eberlein, "Quadriga-quasi deterministic radio channel generator, user manual and documentation," *Fraunhofer Heinrich Hertz Institute, Tech. Rep. v2. 0.0*, 2017.
- [37] J. Liu, Q. Wang, H. Fan, Y. Wang, Y. Tang, and L. Qu, "Residual denoising diffusion models," in *Proceedings of the IEEE/CVF Conference on Computer Vision and Pattern Recognition*, 2024, pp. 2773–2783.

- [38] C. Lu, W. Xu, H. Shen, J. Zhu, and K. Wang, "Mimo channel information feedback using deep recurrent network," *IEEE Communications Letters*, vol. 23, no. 1, pp. 188–191, 2018.
- [39] J. Guo, C.-K. Wen, S. Jin, and G. Y. Li, "Convolutional neural network-based multiple-rate compressive sensing for massive MIMO CSI feedback: Design, simulation, and analysis," *IEEE Transactions on Wireless Communications*, vol. 19, no. 4, pp. 2827–2840, 2020.
- [40] Z. Hu, J. Guo, G. Liu, H. Zheng, and J. Xue, "Mrfnet: A deep learning-based csi feedback approach of massive mimo systems," *IEEE Communications Letters*, vol. 25, no. 10, pp. 3310–3314, 2021.
- [41] X. Chen, C. Deng, B. Zhou, H. Zhang, G. Yang, and S. Ma, "High-accuracy csi feedback with super-resolution network for massive mimo systems," *IEEE Wireless Communications Letters*, vol. 11, no. 1, pp. 141–145, 2021.
- [42] Z. Cao, W.-T. Shih, J. Guo, C.-K. Wen, and S. Jin, "Lightweight convolutional neural networks for csi feedback in massive mimo," *IEEE Communications Letters*, vol. 25, no. 8, pp. 2624–2628, 2021.
- [43] S. Ji and M. Li, "Clnet: Complex input lightweight neural network designed for massive mimo csi feedback," *IEEE Wireless Communications Letters*, vol. 10, no. 10, pp. 2318–2322, 2021.
- [44] Q. Hu, H. Kang, H. Chen, Q. Huang, Q. Zhang, and M. Cheng, "Csi-stripeformer: Exploiting stripe features for csi compression in massive mimo system," in *IEEE INFOCOM 2023-IEEE Conference on Computer Communications*. IEEE, 2023, pp. 1–10.
- [45] B. Wang, F. Gao, S. Jin, H. Lin, and G. Y. Li, "Spatial-and frequency-wideband effects in millimeter-wave massive mimo systems," *IEEE Transactions on Signal Processing*, vol. 66, no. 13, pp. 3393–3406, 2018.
- [46] T. Wang, C.-K. Wen, S. Jin, and G. Y. Li, "Deep learning-based csi feedback approach for time-varying massive mimo channels," *IEEE Wireless Communications Letters*, vol. 8, no. 2, pp. 416–419, 2018.
- [47] O. Ronneberger, P. Fischer, and T. Brox, "U-net: Convolutional networks for biomedical image segmentation," in *Medical image computing and computer-assisted intervention-MICCAI 2015: 18th international conference, Munich, Germany, October 5-9, 2015, proceedings, part III 18*. Springer, 2015, pp. 234–241.
- [48] Z. Li, Y. Zhou, H. Wei, C. Ge, and A. Mian, "Diffusion-based Extreme Image Compression with Compressed Feature Initialization," *arXiv preprint arXiv:2410.02640*, 2024.
- [49] X. Sun, Z. Zhang, and L. Yang, "An Efficient Network with Novel Quantization Designed for Massive MIMO CSI Feedback," *arXiv preprint arXiv:2405.20068*, 2024.
- [50] L. Liu, C. Oestges, J. Poutanen, K. Haneda, P. Vainikainen, F. Quitin, F. Tufvesson, and P. De Doncker, "The cost 2100 mimo channel model," *IEEE Wireless Communications*, vol. 19, no. 6, pp. 92–99, 2012.
- [51] E. TR, "5g; study on channel model for frequencies from 0.5 to 100 ghz," *3GPP TR 38.901 version 16.1. 0 Release 16*, 2020.
- [52] W. Chen, W. Wan, S. Wang, P. Sun, G. Y. Li, and B. Ai, "Csi-ppnet: A one-sided one-for-all deep learning framework for massive mimo csi feedback," *IEEE Transactions on Wireless Communications*, vol. 23, no. 7, pp. 7599–7611, 2023.
- [53] A. Kusupati, G. Bhatt, A. Rege, M. Wallingford, A. Sinha, V. Ramanujan, W. Howard-Snyder, K. Chen, S. Kakade, P. Jain *et al.*, "Matryoshka representation learning," *Advances in Neural Information Processing Systems*, vol. 35, pp. 30 233–30 249, 2022.